Oscillatory dynamics and non-markovian memory in dissipative quantum systems

D.M. Kennes, O. Kashuba, M. Pletyukhov, H. Schoeller, and V. Meden
Institut für Theorie der Statistischen Physik, RWTH Aachen University and
JARA—Fundamentals of Future Information Technology, 52056 Aachen, Germany
(Dated: January 14, 2013)

The nonequilibrium dynamics of a small quantum system coupled to a dissipative environment is studied. We show that (1) the oscillatory dynamics close to a coherent-to-incoherent transition is surprisingly different from the one of the classical damped harmonic oscillator and that (2) non-markovian memory plays a prominent role in the time evolution after a quantum quench.

PACS numbers: 03.65.Yz, 05.30.-d, 72.10.-d, 82.20.-w

To describe dissipation in open quantum systems one often relies on phenomenological approaches. This might be sufficient to model experimental observations as long as the system is large, the coupling to the environment poorly specified, and the accuracy of the measurement limited. The rapid progress in controlled access to small quantum systems in such distinct fields as condensed matter physics, quantum optics, physical chemistry, and quantum information science renders a more microscopic approach inevitable [1, 2].

Two questions of general current interest are: (1) How does the dissipative nonequilibrium dynamics of a quantum system with only a few degrees of freedom compare to the standard example of classical dissipation, the damped harmonic oscillator (DHO)? Do such systems show a coherent-to-incoherent transition of the same type as it is found in the classical case? Studying the time-evolution of the ohmic spin-boson model (SBM) [1, 2] we show analytically that the dynamics in the coherent regime as well as the transition to the incoherent one are surprisingly different from their classical counterparts. (2) What is the role of non-markovian terms in the dynamics of quantum dissipative systems? By considering parameter quenches across the coherent-to-incoherent transition in the SBM we show that non-markovian memory of the state before the quench heavily affects the time evolution after it. When quenching from the incoherent to the coherent regime this effect can be so strong that the dynamics after the quench is monotonic; the coherent oscillatory behavior is fully suppressed. We provide a qualitative analytical explanation of this numerical finding. For quenches in the opposite direction nonmonotonic behavior can be transferred deep into the incoherent part of the dynamics. Recent technological progress to isolate small systems from uncontrolled environmental fluctuations and to manipulate their parameters, e.g. in cold atomic gases, led to a considerable interest in quantum quenches [3]. For the SBM those were not studied so far.

Model—The SBM is arguably the most important model used to describe dissipation in small quantum systems coupled to an environment beyond phenomenological approaches. Its Hamiltonian reads

$$H = \frac{\epsilon}{2}\sigma_z - \frac{\Delta}{2}\sigma_x + \sum_k \omega_k b_k^\dagger b_k - \sum_k \frac{\lambda_k}{2}\sigma_z \left(b_k^\dagger + b_k\right), \quad (1)$$

with the Pauli matrices σ_ν, $\nu = x, z$ and bosonic ladder operators $b_k^{(\dagger)}$. A spin-1/2 with Zeeman splitting ϵ and tunneling $\Delta \geq 0$ between the two states is coupled by λ_k to a reservoir of bosonic modes with dispersion ω_k. The spin-boson coupling is characterized by a spectral density $J(\omega) = \sum_k \lambda_k^2 \delta(\omega - \omega_k)$ given by the details of the microscopic model underlying the SBM [1]. The dynamics was mainly studied in the ohmic case with $J(\omega) = 2\alpha\omega\Theta(\omega_c - \omega)$ and coupling $\alpha \geq 0$ [1, 2, 4–9]. To investigate the fundamental questions raised above we reduce the number of parameters by considering the (symmetric) case $\epsilon = 0$, the scaling limit, with the high-energy cutoff ω_c being much larger than any other scale, and temperature $T = 0$. In this strong-coupling limit the many-body physics becomes most intriguing and any perturbative approach fails [1, 2]. It is established that the time evolution of the spin expectation value [10] $P(t) = \langle\sigma_z(t)\rangle$ changes from being coherent, that is damped oscillatory, for $\alpha < 1/2$ to incoherent, that is monotonic, for $1/2 < \alpha < 1$; at $\alpha = 1$ a quantum phase transition to a localized regime occurs which we do not consider. We show that the coherent regime as well as the transition still offer surprises. Other parameter regimes are investigated in Refs. [11–19].

In studies of the nonequilibrium dynamics the system is often assumed to be in an initial product state of spin-up and the boson vacuum. The time evolution is performed for $\alpha > 0$ and $P(t)$ asymptotically tends to zero. In the following we refer to this setup as the relaxation protocol. We furthermore consider two quench protocols. In the first one the system is prepared in the above initial state and the time evolution is performed with a coupling $2\alpha_i - 1 > 0$ (incoherent regime) up to $t = t_q$. At t_q it is abruptly switched to α_f, with $2\alpha_f - 1 = 1 - 2\alpha_i < 0$ (coherent regime), and the evolution is continued. In the second quench protocol we proceed in opposite order and quench from $2\alpha_i - 1 < 0$ to $2\alpha_f - 1 = 1 - 2\alpha_i > 0$.

Relaxation protocol—The dynamics of the SBM for couplings sufficiently away from the transition at $\alpha = 1/2$

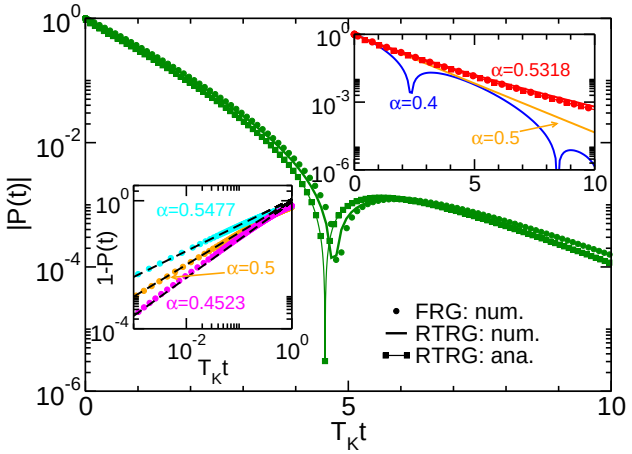

FIG. 1: (Color online) Time evolution of a spin-1/2 prepared in its up state and coupled to an ohmic boson bath at $t = 0$ (spin-boson model). The spin expectation value $|P(t)|$ is shown for different couplings α. Dips correspond to zeros; to make those visible we use a log y-axis scale. Main panel: comparison of the numerical solutions of the FRG and RTRG equations as well as the analytical result Eqs. (2)-(4) for $\alpha = 0.4682$. Right inset: the same as in the main panel (various α; analytical expression for $\alpha = 0.5318$ only for which the curves are barely distinguishable). The dynamics in the coherent regime is very different to that of the classical damped oscillator. Left inset: FRG data for $1 - P(t)$ at short times (dots) compared to the NIBA prediction (dashed lines).

and outside the transient regime, that is for $t\Delta \gtrapprox 1$, is well understood. For small α, that is deep in the coherent regime, it compares well to the one of the classical DHO [7–9, 17] which is given as the sum of terms each being the product of an exponentially damped and an oscillatory factor. Deep in the incoherent regime the dynamics of the SBM is dominated by a single exponentially decaying term [7, 8] in resemblance to that of the DHO.

We now address if the analogy also holds close to the coherent-to-incoherent transition approaching it from the coherent side. For a controlled access to this intruiging regime we employ the smallness of $g = 1 - 2\alpha$. Close to the transition the characteristic low-energy scale $T_K = \Delta\,(\Delta/\omega_c)^{\alpha/(1-\alpha)}$ emerges [1, 2]. For now we take T_K as our unit of energy and measure time in units of T_K^{-1}. Our analytical result for $P(t) = P_{\rm bc}(t) + P_{\rm p}(t)$ at $|g| \ll 1$ and $t \gtrapprox 1$ reads

$$P_{\rm bc}(t) \approx \frac{1}{\pi}{\rm Im}\Big\{e^{-\gamma t}{\rm E}_1\Big(\big[\tfrac{1}{2}\Gamma_2^* - \gamma\big]\,t\Big)\Big\},\quad \gamma = e^{-i\pi g}t^g, \quad (2)$$

$$P_{\rm p}(t) \approx 2\frac{1-g}{1+g}\cos(\Omega t)\,e^{-\Gamma_1^* t}\Theta(g), \quad (3)$$

with

$$\Gamma_2^* \approx 2\left[\frac{\pi g}{2\sin(\pi g)}\right]^{\frac{1}{1+g}},\quad \Omega + i\Gamma_1^* \approx e^{(i\pi + \ln 2)\frac{g}{1+g}} \quad (4)$$

and the exponential integral E_1. It constitutes one of the main results of this Letter. As outlined below it is obtained employing a two-step procedure which is based on complementary renormalization group (RG) approaches: the functional (F) [20] and the real-time (RT) [21] RG. In vast contrast to the dynamics of the classical DHO which on the coherent side shows infinitely many zeros even very close to the coherent-to-incoherent transition $P(t)$ only features a single zero for α close to 1/2. This is exemplified in the main panel of Fig. 1 which shows $|P(t)|$ for $\alpha = 0.4682$ (solid line with symbols); no additional zeros are found for times larger than the ones shown. Our analytical result is compared to the numerical solutions of the differential flow equations (see below) of the FRG (symbols) and the RTRG (solid line). The excellent agreement of all three results indicates that we fully control our approximations (see below). The right inset shows $|P(t)|$ for different α. In the incoherent regime the three curves coincide even better ($\alpha = 0.5318$). For α deeper in the coherent regime further zeros appear, e.g. in total two for $\alpha = 0.4$.

A 'pole contribution' $P_{\rm p}$ Eq. (3) to P is also found in two alternative analytical approaches: the noninteracting blip approximation (NIBA) [1, 2] and conformal field theory (CFT) [6]. Our ratio Ω/Γ_1^* Eq. (4) coincides with the one obtained by these methods [22]. While no 'branch-cut contribution' $P_{\rm bc}$ Eq. (2) appears in CFT [6] the one of NIBA leads to a purely algebraic decay which turned out to be an artifact of this approximation [2]. In Ref. 5 NIBA was improved leading to

$$P_{\rm bc}(t) = -g[1 + 3\Theta(-g)]\frac{e^{-t/2}}{t^{1+|g|}}. \quad (5)$$

This result agrees to our Eq. (2) evaluated for $t^{|g|} \gg 1$ and taking into account that to leading order $\Gamma_2^* \approx 1$ (that is T_K). We emphasize that for $\alpha < 1/2$ the sum of the pole contribution Eq. (3) and the asymptotic result Eq. (5) does not give a meaningful approximation to the dynamics for the times shown in Fig. 1 for which the coherent and incoherent parts are comparable and nonmonotonic ('oscillatory') behavior is found. For those it is inevitable to keep the branch-cut term in the form of Eq. (2). Thus none of the existing analytical approaches to the SBM allows to uncover the crucial difference between the dissipative dynamics of the classical DHO and the SBM close to the coherent-to-incoherent transition. Furthermore, none of the numerical methods applied to the SBM [7–9, 17] was used to investigate the dynamics in the transition region. Most likely the data suffer from numerical noise which prevents to reliably answer subtle questions such as the one of the number of zeros; note that the y-axis of Fig. 1 covers six orders of magnitude.

Further confidence in our RG methods can be gained from considering the short time dynamics $t \lessapprox 1$. For this NIBA predicts [2] $1 - P(t) = t^{1+g}/\Gamma(2+g) + \mathcal{O}(t^{2+2g})$ which favorably compares to our numerical results (left inset of Fig. 1). In fact, within both our RG approaches this expression can be derived analytically as well.

Methods—We next briefly describe our methods. Readers interested in results only can skip this part and still follow the discussion of the quench dynamics below.

Using our RG approaches we do not directly study the SBM but employ the mapping to the fermionic interacting resonant level model (IRLM) [1, 2]. It is sufficient to know that the coupling α of the SBM is related to the two-particle interaction U of the IRLM: $1-2\alpha = 2U - U^2 = g$. The case $\alpha = 1/2$ corresponds to the noninteracting resonant level model ($U = 0$) and is exactly solvable. The FRG flow equations for the Keldysh components of the many-body self-energy of the IRLM derived in Refs. 23 (relaxation protocol) and 24 (quench protocols) are controlled to leading order in U, that is g, and can directly be applied to the SBM.

In the complementary RTRG [21] one focuses on the reduced density matrix of the local system and describes its dynamics in Liouville-Laplace space by

$$P(t) = \frac{i}{2\pi}\int_{-\infty+i0^+}^{\infty+i0^+} dE\, e^{-iEt}\,\Pi_1(E), \tag{6}$$

where $\Pi_1(E) = [E+i\Gamma_1(E)]^{-1}$ is an effective propagator; in the IRLM $\Gamma_1(E)$ denotes the charge relaxation rate. The Laplace variable E can be used as the flow parameter [25], leading to

$$\frac{d\Gamma_{1/2}(E)}{dE} = -g\,\Gamma_1(E)\,\Pi_{2/1}(E), \tag{7}$$

with $\Pi_2(E) = [E + i\Gamma_2(E)/2]^{-1}$ and initial values $\Gamma_n(i\omega_c) = \Delta^2/\omega_c$; in the IRLM $\Gamma_2/2$ describes the level broadening. Solving Eq. (7) offers the unique possibility to identify the singularities of the propagator (poles and branch cuts) in the lower half of the complex plane, from which the individual terms of the time evolution can be identified. The RG equations (7) contain all terms $\mathcal{O}\left(U\frac{\Delta^2}{\omega_c E}\right)$. However, some terms $\mathcal{O}\left(U\left[\frac{\Delta^2}{\omega_c E}\right]^2\right)$ are neglected. This must be contrasted to our FRG approach, which contains all orders in Δ^2/ω_c. To verify that for small $|U|$, that is small $|g|$, considering Eq. (7) is sufficient, we always compare the numerical solutions of the FRG and RTRG flow equations (see Figs. 1-3).

In an analytical solution of our RTRG equations (7) one has to separately consider the branch-cut contribution to the integral Eq. (6) for all g and the pole contributions for $g \geq 0$. The former follows from the branch cut of $\Gamma_1(E)$ on the imaginary axis starting at the pole $-i\Gamma_2^*/2$ of $\Pi_2(E)$. Taking $\Gamma_2(E) \approx \Gamma_2^*$ in $\Pi_2(E)$, we get $\Gamma_1(E) \approx (\Gamma_2^*/2 - iE)^{-g}$ from Eq. (7), leading to

$$P_{\rm bc}(t) = -\frac{e^{-\Gamma_2^* t/2}}{\pi}\int_0^\infty dx\,{\rm Im}\left\{\frac{e^{-xt}}{\frac{\Gamma_2^*}{2} + x - e^{i\pi g}x^{-g}}\right\}. \tag{8}$$

Replacing x^g by t^{-g} in the denominator gives a very good approximation for $t \gtrapprox 1$ and leads to Eq. (2). A comparison with the numerical solution shows that to find the pole positions $z_1 = \pm\Omega - i\Gamma_1^*$ ($z_2 = -i\Gamma_2^*/2$) of $\Pi_1(E)$ ($\Pi_2(E)$) one can set $\Gamma_1(E) \approx \Gamma_2(E) \approx iz_1$ ($\Gamma_1(E) \approx \Gamma_2(E) \approx \Gamma_2^*$) in $\Pi_n(E)$. The RG equations can then be solved analytically leading to Eq. (4) as well as the pole contribution to $P(t)$ Eq. (3).

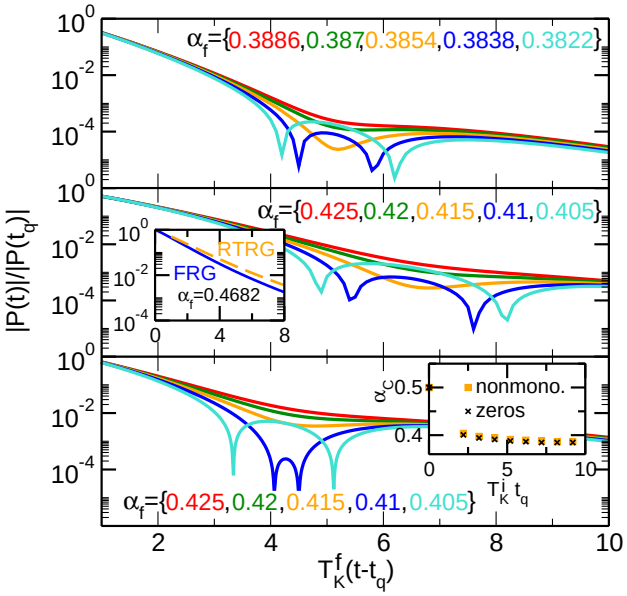

FIG. 2: (Color online) Spin expectation value $P(t)$ of a spin-1/2 with the initial time evolution given by the spin-boson Hamiltonian and a coupling from the incoherent regime $\alpha_i > 1/2$. At $t = t_q$ it is switched to $\alpha_f < 1/2$ from the coherent one. The scaling limit is realized by $\Delta/\omega_c = 1/200$. Times are restricted to $t > t_q$; for $0 < t < t_q$, see Fig. 1. Left inset: comparison of numerical FRG and RTRG data; the non-markovian memory completely suppresses the coherent 'oscillatory' behavior. It only survives for α_f smaller than a critical coupling α_c; see the upper [numerical solution of FRG equations], central [numerical solution of RTRG equations], and lower [analytical result Eq. (10)] panels. Right inset: dependence of α_c on the time $T_K^i t_q$ the evolution was performed in the incoherent regime (FRG data). Two different definitions of α_c are compared. In the first α_c is defined as the α_f at which the first zero of $P(t)$ can be observed, in the second as the α_f at which the curve first shows a nonmonotonicity. The two values barely differ.

Quench protocol 1—We next investigate the role of non-markovian memory in dissipative dynamics. In Fig. 2 we show $P(t)$ when quenching at t_q from the incoherent to the coherent regime. The two different couplings α_i and α_f lead to the two characteristic scales T_K^i and T_K^f, which in the scaling limit differ by orders of magnitude. Therefore the model parameters Δ and ω_c cannot be scaled out as efficiently as in the relaxation protocol (by taking T_K as the unit of energy). To minimize the influence of the transient dynamics before the quench we consider $T_K^i t_q$ between 5 and 10. In the left inset we compare the data obtained by the numerical solution of the FRG [24] and RTRG equations (see

below). The agreement for $\alpha_{i/f}$ close to 1/2 is excellent. Even though the same coupling $\alpha_f = 0.4682$ as in the main panel of Fig. 1 is considered the data for the quench dynamics displayed in the left inset of Fig. 2 are monotonic; no indication of coherent behavior is found. The incoherent dynamics before the quench thus heavily affects the one afterwards. To further investigate this, results for smaller α_f are shown in the upper (FRG) and central (RTRG) panel. Nonmonotonic ('oscillatory') behavior can only be found for α_f being smaller than some critical coupling α_c. As $|1 - 2\alpha_c| \ll 1$ does not hold strictly, our two approximate RG methods give values for α_c which differ by a few percent. Its precise value can only be obtained using a method which treats higher order contributions consistently.

Quenches were so far not studied using RTRG; the technical details will be given elsewhere. In this approach the memory of the spin state is preserved in the excitations of the bath. Classifying the memory contributions by the number of bath excitations that have gone through the quench one can show that the terms with n excitations are proportional to $A^n = (T_K^i/T_K^f)^{n/2} \approx (\Delta/\omega_c)^{2n|g_f|}$, with $A \ll 1$. Restricting ourselves to the case of a single excitation with Matsubara frequency Λ we obtain ($t' = t - t_q \geq 0$)

$$P(t') = P^f(t')P^i(t_q) - g_i \int_0^\infty d\Lambda F_\Lambda^f(t') F_\Lambda^i(t_q), \qquad (9)$$

$$F_\Lambda^\kappa(t) = -\int_{-\infty}^{\infty} \frac{dE}{2\pi} e^{-iEt} \Pi_1^\kappa(E + i\Lambda) \sqrt{\Gamma_1^\kappa(E)} \Pi_2^\kappa(E)$$

with $\kappa = i, f$ and P^κ, $\Gamma_{1/2}^\kappa$ computed as in the relaxation protocol with the corresponding $\alpha_{i/f}$ and initial condition $P^\kappa(0) = 1$. The first term describes standard relaxation while the second memory term implies (dissipative) non-markovian dynamics. It has no analog for quenches in closed systems. The RTRG data of Fig. 2 were obtained by numerically performing the E and Λ integrals in Eq. (9) on the basis of the numerical solution of Eq. (7). Fixing ω_c the results depend only very weakly on Δ^2/ω_c (via A). Varying $(\Delta/\omega_c)^2$ by an order of magnitude around the average value $2.5 \cdot 10^{-5}$ results in a change of α_c by only a few percent.

To gain qualitative analytical insight of the interplay of the relaxation dynamics and the non-markovian correction we evaluate the integrals keeping only the terms which dominate for $|g_{i/f}| \ll 1$. The result

$$\frac{P(t')}{P(t_q)} \approx 2(1 - A) e^{-\Gamma_1^{*f} t'} \cos(\Omega^f t') + A e^{-\Gamma_2^{*f} t'/2} \qquad (10)$$

is shown in the lower panel of Fig. 2. The memory generates a coherent and an incoherent contribution $\propto A$. The first has a negative sign and suppresses the coherent part while the second enhances the incoherent term compared to the one of the relaxation protocol; for $g_f \ll 1$ the latter is subdominant and thus not written in Eq. (10). This explains the appearance of a critical α_c.

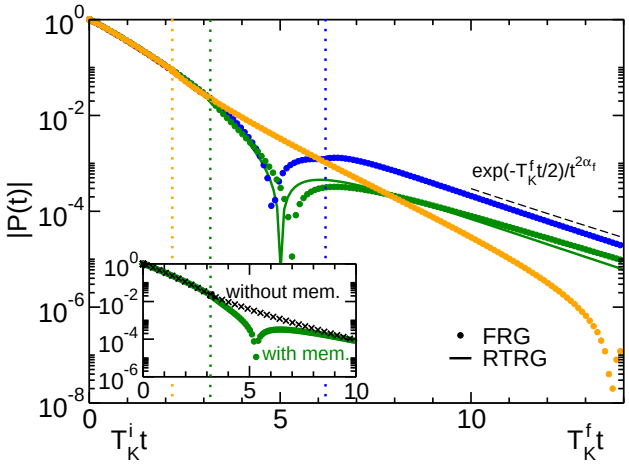

FIG. 3: (Color online) The same as in Fig. 2 but for quenches from the coherent to the incoherent regime. The spin expectation value $|P(t)|$ for $\alpha_i = 0.4682$ and different quench times t_q (indicated by the vertical dotted lines) is shown. At the respective t_q the x-axis scale is switched from $T_K^i t$ to $T_K^f t$. Main panel: data of the numerical solutions of the FRG and RTRG flow equations. The thin dashed line is an exponential term with rate $T_K^f/2$ and a subleading power-law correction. Inset: FRG data with and without the memory term. The non-markovian memory leads to a transfer of nonmonotonic behavior deep into the incoherent part of the dynamics.

Quench protocol 2—We finally discuss the dynamics when quenching at t_q in the opposite direction, that is from the coherent to the incoherent regime. To keep the discussion transparent we focus on α_i's for which only a single zero at time t_0 is found in the relaxation protocol. In Fig. 3 we show $|P(t)|$ obtained from the numerical solution of FRG and RTRG equations for $\alpha = 0.4682$. In the relaxation protocol $T_K t_0 \approx 5$ for this coupling (see Fig. 1). Different quenching times t_q are considered. For $t_q > t_0$ the dynamics at times larger than t_q very quickly adapts to the new rate $\approx T_K^f/2$ of the incoherent dynamics [see Eq. (5) and the dashed line in Fig. 3]. The behavior is significantly different for $t_q < t_0$. In this case nonmonotonic ('oscillatory') behavior is found for times $t > t_q$ at which the time evolution is performed with $\alpha_f = 0.5318 > 1/2$. The smaller $t_q - t_0$ the further the memory term (see the inset of Fig. 3) transfers the zero into the incoherent regime.

Summary—We have shown that the coherent dynamics of the ohmic SBM, being the prototype model of dissipative quantum mechanics, close to the coherent-to-incoherent transition is very different from the one of the classical DHO. Our study furthermore revealed the crucial importance of non-markovian memory in the nonequilibrium time evolution when quenching across this transition. Both these findings come as surprises.

Acknowledgments—This work was supported by the DFG via FOR 723. We thank R. Egger, C. Karrasch, and U. Weiss for discussions.

[1] A.J. Leggett, S. Chakravarty, T.A. Dorsey, M.P.A. Fisher, A. Garg, and W. Zwerger, Rev. Mod. Phys. **59**, 1 (1987).

[2] U. Weiss, *Quantum Dissipative Systems* (World Scientific Publishing Company, Singapore, 2012).

[3] A. Polkovnikov, K. Sengupta, A. Silva, and M. Vengalattore, Rev. Mod. Phys. **83**, 863 (2011).

[4] R. Egger and C.H. Mak, Phys. Rev. B **50**, 15210 (1994).

[5] R. Egger, H. Grabert, and U. Weiss, Phys. Rev. E **55**, R3809 (1997).

[6] F. Lesage and H. Saleur, Phys. Rev. Lett. **80**, 4370 (1998).

[7] F.B. Anders and A. Schiller, Phys. Rev. B **74**, 245113 (2006).

[8] H. Wang and M. Thoss, New J. Phys. **10**, 115005 (2008).

[9] P.P. Orth, A. Imambekov, and K. Le Hur, Phys. Rev. A **82**, 032118 (2010).

[10] P is equivalent to the population imbalance when viewing the SBM as a two-level system [1, 2].

[11] M. Grifoni and P. Hänggi, Phys. Rep. **304**, 229 (1998).

[12] M. Keil and H. Schoeller, Phys. Rev. B **63**, 180302 (2001).

[13] D.P. DiVincenzo and D. Loss, Phys. Rev. B **71**, 035318 (2005).

[14] A. Hackl and S. Kehrein, Phys. Rev. B **78**, 092303 (2008).

[15] A. Alvermann and H. Fehske, Phys. Rev. Lett. **102**, 150601 (2009).

[16] P.P. Orth, D. Roosen, W. Hofstetter, and K. Le Hur, Phys. Rev. B **82**, 144423 (2010).

[17] P.P. Orth, A. Imambekov, and K. Le Hur, arXiv:1211.1201

[18] Kast, Denis and Ankerhold, Joachim, Phys. Rev. Lett. **110**, 010402 (2013).

[19] Kast, Denis and Ankerhold, Joachim, arXiv:1301.1772

[20] W. Metzner, S. Salmhofer, C. Honerkamp, V. Meden, and K. Schönhammer, Rev. Mod. Phys. **84**, 299 (2012).

[21] H. Schoeller, Eur. Phys. J. Spec. Top. **168**, 179 (2009).

[22] The prefactor of $P_{\rm p}(t)$ Eq. (3) agrees with the one of NIBA only to order g^0. We were informed by U. Weiss that computing it within improved NIBA [5] gives a result which agrees to ours to order g.

[23] D.M. Kennes, S.G. Jakobs, C. Karrasch, and V. Meden, Phys. Rev. B **85**, 085113 (2012).

[24] D.M. Kennes and V. Meden, Phys. Rev. B **85**, 245101 (2012).

[25] M. Pletyukhov and H. Schoeller, Phys. Rev. Lett. **108**, 260601 (2012).